

Electrophoretic and quasi-elastic light scattering of soluble protein-polyelectrolyte complexes

Jiulin Xia, Paul L. Dubin, Yesook Kim, Barry B. Muhoberac, and Valentine J. Klimkowski

J. Phys. Chem., **1993**, 97 (17), 4528-4534 • DOI: 10.1021/j100119a046 • Publication Date (Web): 01 May 2002

Downloaded from <http://pubs.acs.org> on February 14, 2009

More About This Article

The permalink <http://dx.doi.org/10.1021/j100119a046> provides access to:

- Links to articles and content related to this article
- Copyright permission to reproduce figures and/or text from this article



ACS Publications
High quality. High impact.

Electrophoretic and Quasi-Elastic Light Scattering of Soluble Protein–Polyelectrolyte Complexes

Julin Xia,^{*†} Paul L. Dubin,^{*†} Yesook Kim,[‡] Barry B. Muhoberac,[†] and Valentine J. Klimkowski[§]

Department of Chemistry, Indiana University–Purdue University at Indianapolis, Indianapolis, Indiana 46205, and Parenteral Research and Development, and Super Computer Applications and Molecular Design, Eli Lilly & Company, Indianapolis, Indiana 46285

Received: September 15, 1992; In Final Form: November 30, 1992

Complexation between globular proteins (bovine serum albumin, bovine pancreas ribonuclease, and chicken egg lysozyme) and a number of synthetic polyelectrolytes was studied by quasi-elastic light scattering (QELS) and electrophoretic light scattering in dilute electrolyte solution. For each polyion–protein pair, there is a well-defined critical pH at which binding commences (pH_c). At this pH, QELS reveals fast and slow diffusion modes corresponding to free protein and complex, respectively; the relative amplitude of the latter increases with pH in the case of polycations, with opposite pH dependence for polyanions. Further pH change produces phase separation at a second well-defined point (pH_ϕ). The electrophoretic mobility of the polymer begins to change at pH_c and moves toward zero as pH approaches pH_ϕ . These results are discussed in terms of (1) the role of protein “charge patches” as binding sites and (2) the alternative possibilities of intra- and inter-polyion complex formation.

Introduction

Proteins interact strongly with natural and synthetic polyelectrolytes, mainly through electrostatic forces. These forces may lead to the formation of soluble complexes,^{1,2} complex coacervates,^{3–6} and amorphous precipitates.^{7–9} Early studies of protein–polyelectrolyte complex formation were carried out by Morawetz et al.^{10,11} in the 1950s. These studies describe the precipitation of liver catalase by some synthetic polyelectrolytes. Subsequently, the purification of proteins by polyelectrolytes was proposed. So far, protein–polyelectrolyte precipitation has been successfully used to separate and isolate whey proteins, to fractionate egg white proteins, and to remove nucleic acids from Baker's yeast.^{12–14} Beside the application of polyelectrolytes to protein purification,^{15–17} polyelectrolytes have also been found to inhibit enzymatic activity of some proteins.^{18,19} Some synthetic polyelectrolytes have recently been shown to have significant inhibitory effects on bacteria, fungi, viruses, tumors, and enzymes when given to test animals prior to viral or tumoral challenge.^{20,21} Finally, understanding the details of these interactions at the molecular level may help clarify the mechanism of protein–nucleic acid approach and binding. For such varied reasons, studies of the interactions between synthetic polyelectrolytes and proteins could clarify the fundamental roles of the polyelectrolyte in *inter alia* protein purification, enzyme activity modification, and host resistance to a variety of pathophysiology.

An understanding of the properties of macroscopic protein–polyelectrolyte complexes requires insight into the formation and structure of soluble complexes. On the basis of studies of the complexation of bovine serum albumin (BSA) and quaternized poly(4-vinylpyridines), Kabanov²² proposed a model in which the polycation is wound around an asymmetrical, approximately cylindrical stack of BSA molecules. A number of free polyion loops maintain a hydrophilic zone along the surface of the stack promoting the solubility of the particles of the complex. More recently, Dubin et al.¹⁶ studied the complexation of poly(dimethyldiallylammonium chloride) (PDMDAAC) with different proteins and proposed the existence of a “primary” soluble complex in which a single polymer chain encompasses and entraps a number of proteins.

Quasi-elastic light scattering (QELS) and electrophoretic light scattering (ELS) have proven to be powerful techniques in the study of macromolecular solutions.^{23,24} However, the application of QELS to the study of protein–polymer complexation is quite recent,^{16,25,26} and the corresponding use of ELS has not been explored to the best of our knowledge. In this study, we use QELS and ELS techniques to study the association behavior of proteins with polyelectrolytes of different linear charge densities as part of a continuing effort to understand interactions and structure in protein–polyelectrolyte systems.²⁷

Experimental Section

Materials. Structures of the synthetic cationic and anionic polymers are shown in Figure 1. Poly(dimethyldiallylammonium chloride) (PDMDAAC) was a commercial sample of “Merquat 100” from Calgon Corporation (Pittsburgh, PA), possessing a nominal molecular weight (MW) of 2×10^5 and having a reported polydispersity of $M_w/M_n \geq 10$. (Because of an earlier controversy concerning the interpretation of NMR spectra, PDMDAAC was previously thought by us and others to contain a six-membered ring as a repeating unit.) LBN 52b, a homopolymer of the acrylate of (trimethylamino)ethyl chloride (CMA), and LBN 66 (50% of CMA with acrylamide) were both kindly supplied by Dr. F. Lafuma from the laboratory of Dr. R. Audebert, University Pierre et Marie Curie, Paris.²⁸ The values of M_w for LBN66 and LBN52b are 5.6×10^5 and 2×10^5 , respectively, and the polydispersities are estimated at ca. 2 from size exclusion chromatography.²⁹ Sodium poly(styrenesulfonate) (NaPSS) was from Pressure Chemical Company (Pittsburgh, PA) with nominal MW of 354 000, and polydispersity of less than 1.1, and used as received.³⁰ Sodium poly(vinyl sulfate) (PVS) with nominal MW 2000 was obtained from Polyscience Inc. (Warrington, PA) as a 5% aqueous solution. Sodium poly(2-acrylamidomethylpropyl sulfate) (PAMPS) and the copolymer of AMPS with *N*-vinylpyrrolidone (50 mol %) (NVP-AMPS), with MWs of 2.4×10^6 and 2×10^6 , respectively,³¹ were prepared by free radical polymerization by D. W. McQuigg of Reilly Industries (Indianapolis, IN). The polydispersities of PVS, PAMPS, and NVP-AMPS were not determined. Bovine serum albumin (BSA), bovine pancreas ribonuclease (RNase), and chicken egg lysozyme were obtained from Sigma Chemical as 95–99% pure lyophilized proteins, with *pI* values of 4.9, 9.0, and 11.0, respectively.

Sample Preparation. All solutions were prepared with deionized water that was made from glass distilled water subsequently passed

^{*} Indiana University–Purdue University at Indianapolis.

[†] Parenteral Research and Development, Eli Lilly & Co.

[§] Super Computer Applications and Molecular Design, Eli Lilly & Co.

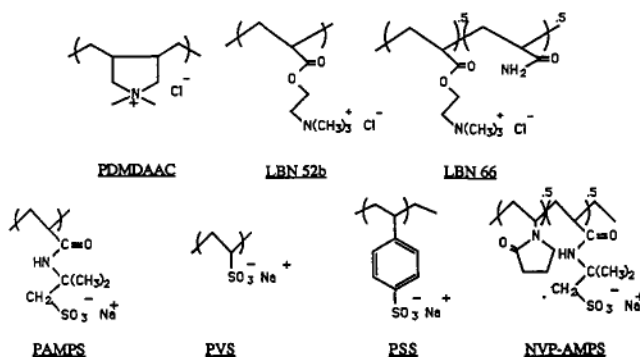


Figure 1. Molecular structures of the polyelectrolytes.

through one carbon and two ion-exchange filters. Scattering solutions were made dust-free by filtration through 0.2- μm Acrodisc filters. The concentrations of protein and polyelectrolyte in $I = 0.1$ M NaCl solution were 5 and 1 g/L, respectively. These concentrations correspond to excess protein concentration in terms of the number of proteins per polymer chain,¹⁶ except for the case of the very low MW PVS where the number of polymer chains is greater than that of proteins. The salt concentration was selected so as to maintain constant ionic strength irrespective of pH adjustment, without being large enough to reduce the intrinsic protein solubility.

Methods. Quasi-Elastic Light Scattering. Quasi-elastic light scattering measurements were made at scattering angles from 30° to 150° with a Brookhaven (Holtville, NY) 72-channel BI-2030 AT digital correlator and using a Jodon 15-mW He-Ne laser (Ann Arbor, MI). We obtain the homodyne intensity-intensity correlation function $G(q,t)$, with q , the amplitude of the scattering vector, given by $q = (4\pi n/\lambda) \sin(\theta/2)$, where n is the refractive index of the medium, λ is the wavelength of the excitation light in a vacuum, and θ is the scattering angle. $G(q,t)$ is related to the time correlation function of concentration fluctuations $g(q,t)$ by

$$G(q,t) = A(1 + bg(q,t)^2) \quad (1)$$

where A is the experimental base line and b is a constant related to the fraction of the scattered intensity arising from concentration fluctuations. The quality of the measurements was verified by determining that the difference between the measured value of A and the calculated one was less than 1%. More detailed discussions of QELS data analysis may be found in refs 32 and 33.

In general, the correlation function can be expressed as an integral sum of exponential decays weighted over the distribution of relaxation times $\rho(\tau)$:

$$\left[\frac{G(t) - A}{A} \right]^{1/2} = b^{1/2} g(t) = \int_0^\infty e^{-t/\tau} \rho(\tau) d\tau \quad (2)$$

In principle, it is possible to obtain the distribution $\rho(\tau)$ by integral transformation of the experimental $[G(t)/A - 1]^{1/2}$, but in practice this presents a formidable problem for numerical analysis, since taking the inverse Laplace transform is numerically an ill-posed problem. Several numerical methods developed so far are devoted to calculating $\rho(\tau)$. In the present work, we analyze the autocorrelation functions by using the CONTIN program, which employs the constrained regularization method.³⁴

From eq 2, the mean relaxation time, $\langle \tau \rangle$, defined as the area of $g(t)$, is given by

$$\begin{aligned} \langle \tau \rangle &= \int_0^\infty g(t) dt \\ &= \int_0^\infty \tau \rho(\tau) d\tau / \int_0^\infty \rho(\tau) d\tau \quad (3) \end{aligned}$$

This $\langle \tau \rangle$ value can be resolved from each of the distribution modes of $\rho(\tau)$, as the first moment of the normalized relaxation spectrum. Therefore, the diffusion coefficient, which corresponds

to each value of $\langle \tau \rangle$, can be calculated using

$$D = \frac{\lambda^2}{16\pi^2 \sin^2(\theta/2) \langle \tau \rangle} \quad (4)$$

From each D value we obtain the Stokes radius, R_s , by the Einstein equation

$$R_s = kT/6\pi\eta D \quad (5)$$

where k is the Boltzmann constant, T is the absolute temperature, and η is the viscosity of the solvent.

Electrophoretic Light Scattering. Electrophoretic light scattering (ELS) measurements were made at 25 °C and four scattering angles (8.6°, 17.1°, 25.6°, and 34.2°), using a Coulter (Hialeah, FL) DELSA 440 apparatus. The electric field was applied at a constant current of 5 mA.

In ELS, the photon-counting heterodyne correlation function for a solution with an electrophoretically monodisperse solute can be written as³⁵

$$C(\tau) = \beta_0 \delta(\tau) + \alpha_0 + \alpha_1 \exp(-2Dq^2\tau) + \alpha_2 \exp(-Dq^2\tau) \cos(\Delta\omega\tau) \quad (6)$$

where β_0 , α_0 , α_1 , and α_2 are constants independent of correlation time, τ , and $\delta(\tau)$ is the delta function. D and q have the same definitions as in QELS. The cosine term is due to simultaneous electrophoresis and diffusion.

The Fourier transform of eq 6 with respect to time, as stipulated by the Wiener-Khinchine theorem,³⁶ gives the power spectrum:

$$S(\omega) = \beta_0 + \alpha \delta(\omega) + \frac{2(\alpha_1/\pi)Dq^2}{\omega^2 + (2Dq^2)^2} + \frac{\alpha_2 Dq^2}{2\pi} \times \left[\frac{1}{(\omega + \Delta\omega)^2 + (Dq^2)^2} + \frac{1}{(\omega - \Delta\omega)^2 + (Dq^2)^2} \right] \quad (7)$$

where α is a constant independent of ω .

In both eqs 6 and 7, $\Delta\omega$ is the difference between the angular frequency of the scattered light, ω_s , and that of the reference beam, ω_r , which is the same as that of the incident beam. Since the frequency of the incident beam is modulated in the scattered light by the amount of the so-called Doppler shift frequency, $\Delta\omega$ is given by

$$\Delta\omega = (2\pi n/\lambda)Eu \sin \theta \quad (8)$$

where E (V/cm) and u ($\mu\text{m s}^{-1}$)/(V cm^{-1}) are the applied electric field strength and electrophoretic mobility, respectively. Therefore, u can be directly evaluated from frequencies of the power spectrum. Detailed discussion on ELS measurements can be found in several reviews.^{32,35,37}

Electrostatic Potential Calculations. The molecular system was prepared and the calculations were set up using version 3.2 of the program QUANTA and version 21.3 of CHARMM,^{38,39} running on an SGI Indigo, XS24 workstation. Coordinates for RNase were those refined by Wlodawer et al.⁴⁰ and deposited as data set "5rsa" in the Brookhaven Protein Databank.⁴¹ Although the coordinates of many of the protein's hydrogens had been determined by neutron diffraction, for the purpose of this study these and the crystallographic waters were removed. Polar hydrogens were added and their positions initially optimized using the HBUILD facility⁴² of CHARMM. These were further refined by fixing the positions of all but the hydrogen atoms and applying 55 steps steepest descents followed by 100 steps adopted basis Newton-Raphson energy minimization. The active site phosphate group was maintained with a -3 total charge. All basic, acidic, and terminal residues were represented as fully charged. Histidines were initially considered to be neutral. However, on close examination of all four histidines present, it was determined that if those at positions 12 and 119 were the charged species, additional hydrogen bonds would be created that help stabilize the phos-

TABLE I: Apparent Diameters of the Proteins and Polyelectrolytes in 0.10 M NaCl^a

polymer	d_s (nm)	polymer	d_s (nm)	polymer	d_s (nm)
NaPVS	6 ^b	PDMDAAC	20	BSA	8.0
NaPSS	46	LBN 52	28	RNase	6.0
PAMPS	30	LBN 66	31	lysozyme	4.0
NVP-PAMPS	40				

^a Obtained at the same solute concentrations employed in studies of the mixed systems: 1.0 g/L for polymer, 5.0 g/L protein. ^b Measured at 8 g/L (weak scatterer).

TABLE II: Geometric Charge Densities and Mobilities of the Polyelectrolytes

polymer	GCD	u [($\mu\text{m cm}$)/ $(\text{V s})]$	polymer	GCD	u [($\mu\text{m cm}$)/ $(\text{V s})]$
polyanions			polycations		
NaPVS	-0.034	-2.92	PDMDAAC	0.008	1.61
NaPSS	-0.01	-2.04	LBN 52	0.01	1.98
PAMPS	-0.01	-1.82	LBN 66	0.005	1.08
NVP-PAMPS	-0.005	-1.22			

phonate group. This change was made and all hydrogen positions redefined as described above.

The electrostatic potential surrounding RNase was calculated by the linearized Poisson-Boltzmann equation using the finite difference method as embodied in the program UHBD,⁴³ version 2.2. This was performed with dielectric constants of 2 for the protein interior and 78 for the solvent region. An ionic strength of 0.0 mM was used and the temperature set to 300 K. With the protein centered in a cube having a length of 53 Å per side, the electrostatic potential was evaluated in the solvent region at each point on a superimposed grid having a spacing of 1.5 Å.

Results and Discussion

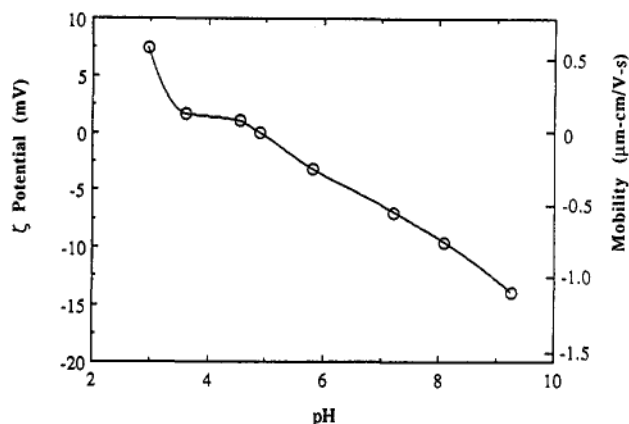
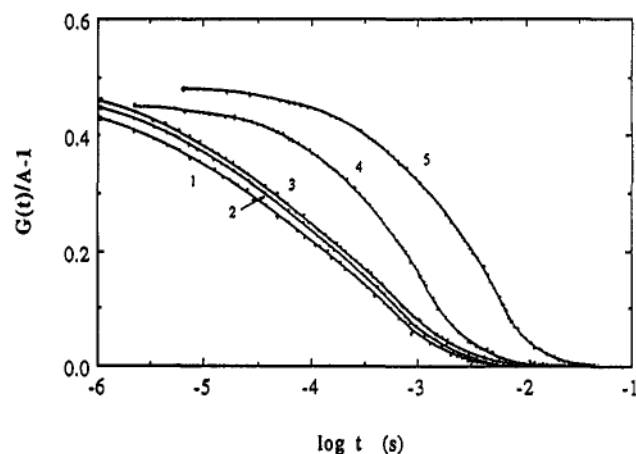
Light Scattering Characterization of Uncomplexed Polyelectrolytes and Proteins. In order to characterize the complexation of polyelectrolytes and proteins, QELS measurements of the separate polyelectrolytes and proteins were carried out. The apparent diameters of the polymers and proteins are shown in Table I. These QELS measurements were carried out at the same conditions as in the complex solution, in order to identify the point of initial size increase. Since the low MW (2000) PVS is a very weak scatterer, QELS was carried out at a relatively high concentration of ca. 8 mg/mL. Especially in this case, the apparent size is not the true hydrodynamic radius, which would be obtained by extrapolating to zero concentration. The nominal MW = 2000 provided by the supplier of this material may also be questioned. The stability of BSA, RNase, and lysozyme over the present range of conditions was verified in our previous study.²⁷

Besides the apparent size, the electrophoretic mobility is another important quantity by which charged particles are characterized. The electrophoretic mobility data for the pure polyelectrolytes are given in Table II. In this table the "geometric surface charge densities" (GCD) of the polymers are also listed. The GCD values were calculated employing part of the model of Davis and Russell in which the polyanion is treated as a cylinder bearing a continuous smeared charge.⁴⁴ In Table II it is interesting to note that the measured mobilities monotonically increase with the calculated GCD values. This result may be considered in terms of the Debye-Hückel theory. If we use the ζ potential as an approximation of the surface potential ϕ of a uniformly charged sphere, the theory gives

$$\zeta \approx \phi = 4\pi(\sigma/\epsilon\kappa) \quad (9)$$

where σ is the surface charge density of the particle, and ϵ and κ are the dielectrical constant and Debye-Hückel parameter of the solution, respectively. The relationship between the mobility (u) and the ζ potential is

$$\zeta = 4\pi(\eta u/\epsilon) \quad (10)$$

**Figure 2.** Electrophoretic mobility and ζ potential of BSA as a function of pH in 0.10 M NaCl.**Figure 3.** Autocorrelation functions of LBN 66-lysozyme complex obtained at $\theta = 90^\circ$ in 0.10 M NaCl at various pH: (1) 8.07; (2) 8.45; (3) 8.96; (4) 9.62; and (5) 10.09.

Then, u can be written as

$$u = \sigma/\eta\kappa \quad (11)$$

where η is the viscosity of the solution. Since the polyelectrolytes are in random coil conformations, the quantitative application of eq 9 is not expected. However, it has been shown experimentally that the mobility of a polyelectrolyte is identical to the mobility of the polymer unit, as given by^{23,24}

$$u = q_0/f_0 \quad (12)$$

where q_0 and f_0 are the charge and friction of the polymer unit, respectively. Since the friction factor f_0 is proportional to the unit size, the proportionality of u to the charge density (charge per unit size) as seen in Table II is expected.

Unlike polyelectrolytes, proteins form globular structures in solution and their charge varies with pH. Figure 2 shows both the electrophoretic mobility and ζ potential of BSA in 0.10 M NaCl solution as a function of pH. The ζ potentials were calculated from the measured mobilities using eq 10. The electrophoretic mobility of BSA in different buffer solutions has been reported.³⁵ However, this is, to the best of our knowledge, the first study of BSA mobility by ELS over such a wide pH range. Since the mobility is equal to the protein charge divided by the friction factor, the zero mobility obtained at pH 4.90 is consistent with the known isoelectric point of the protein.

Quasi-Elastic Light Scattering Study of the Complexation Process. Shown in Figure 3 are the autocorrelation functions of solutions of LBN 66-lysozyme at $\theta = 90^\circ$ and different pH values. The dots are experimental points, and the solid lines are the CONTIN fits. The distribution functions, $\rho(\tau)$, calculated for the solutions are plotted in Figure 4 as a function of relaxation time. It is clear that $\rho(\tau)$ changes with pH from a single mode

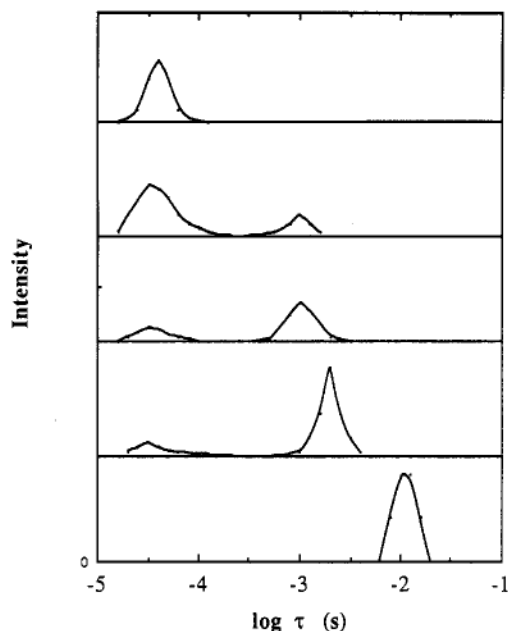


Figure 4. Distribution functions of LBN 66-lysozyme complex obtained by CONTIN program from the autocorrelation functions at different pH (corresponding net protein charge): 8.07 (+6.4), 8.45 (+6.0), 8.96 (+5.7), 9.62 (+4.7), and 10.09 (+1.0) (from top to bottom).

to a bimodal distribution. To make sure that both relaxation times resolved by CONTIN are due to diffusion, we carried out angular dependence measurements, as shown in Figure 5 for LBN 66-lysozyme at pH 8.96. The observation that the curves in Figure 5 for both fast and slow modes of relaxation are linear and with zero intercept confirms that the bimodal distribution corresponds to two diffusion modes.

The diffusion due to pure polyelectrolyte was not resolved because of the low polyelectrolyte concentration and because the refractive index of the polymer is close to that of the solvent (see Figure 4). At $\text{pH} \leq 8.07$, one diffusion mode was resolved with a relaxation time constant identical to that of the pure protein. The bimodal distribution was first resolved at $\text{pH} 8.50$, with a fast mode of the same relaxation time as the single distribution observed at $\text{pH} \leq 8.07$. While the fast mode decreases in intensity with increasing pH, the slow mode increases with respect to both intensity and relaxation time. The slow modes have slower diffusion than that of the polymer. These results suggest that the bimodal distribution corresponds to the diffusion of the pure protein and the complex formed by the protein and the polymer. The onset of slow modes corresponding to complex formation is defined as pH_c^q (or Z_c^q in terms of net protein charge). With increasing pH, binding and soluble complex formation are enhanced. At $\text{pH} 10.02$, the fast mode disappears and the solution becomes cloudy, corresponding to phase separation. This phase separation is initiated by a colloidal solution, which does not at once form two totally separate phases. The colloidal particles aggregate over a period of time without further change in pH. This pH is defined as pH_ϕ (phase separation pH) (or Z_ϕ). The

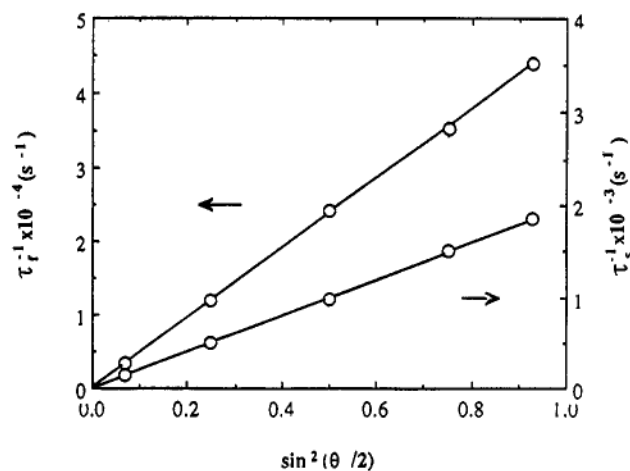


Figure 5. Relaxation time constants of LBN 66-lysozyme system as a function of $\sin^2(\theta/2)$ at pH 8.96 and 0.10 M NaCl.

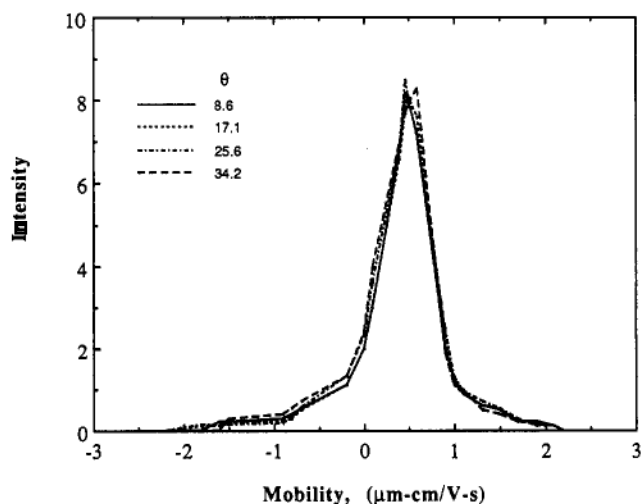


Figure 6. Electrophoretic light scattering spectra of RNase-LBN 66 complex obtained in 0.10 M NaCl at pH 9.10 and scattering angles 8.6° , 17.1° , 25.6° , and 34.2° .

Z_c^q and Z_ϕ values so obtained for various proteins and polymers are shown in Table III.

The range of diameters of soluble complexes for various pairs of proteins and polymers is shown in Table IV. One notes that in each case the initial observed complex at pH_c^q has a size similar to that of the corresponding polymer and that the final soluble complex at $\text{pH} \leq \text{pH}_\phi$ has more than twice this diameter. (The sizes corresponding to pH_ϕ were measured for the colloidal solution, at the point of incipient phase separation, prior to physical coacervation.) This suggests that the initial complex may have an intra-polymer structure ("primary complex"), which then self-aggregates to inter-polymer complex en route to coacervation. Static light scattering studies of the soluble complex formed between BSA and PDMDAAC support this hypothesis.⁴⁵

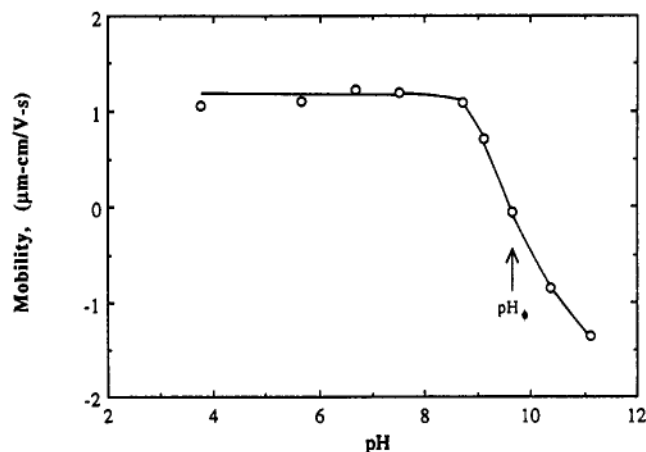
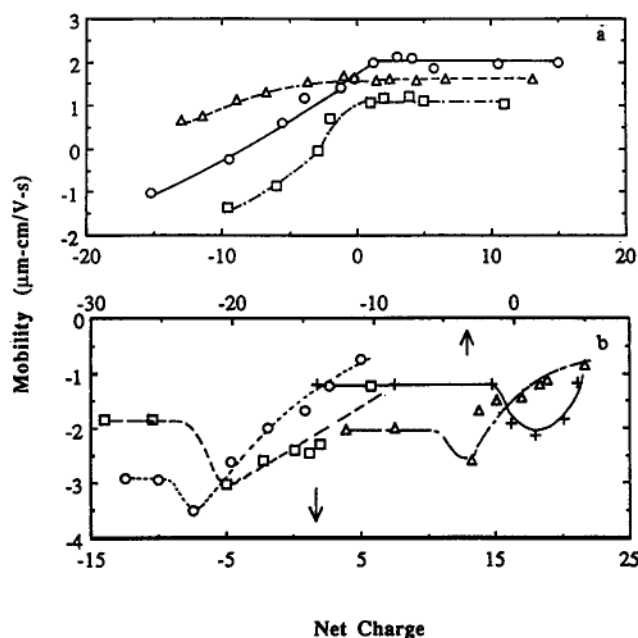
TABLE III: Net Protein Charge at Initial Polymer Binding (Z_c^q)^a and Phase Separation (Z_ϕ)

	BSA			RNase			lysozyme		
	Z_c^q	Z_c^e	Z_ϕ	Z_c^q	Z_c^e	Z_ϕ	Z_c^q	Z_c^e	Z_ϕ
polyanions									
NVP-AMPS	-6	-8	+4	-2	-1.5	+3.5	-1.6	-1.0	+2
NaPSS	-12	-12	-1	-3	-3	+5	-2.6	-1.7	+0.7
PAMPS	-14	-15	-2	-4	-5	+2	-2.6	-2.5	+1.3
NaPVS	-25	-26	+3	-8	-7.5	+5	-7	-6.5	+1.3
polycations									
LBN 66	-2	-2	-30	-3	-2	-6	+6	+6	+1
PDMDAAC	-6	-5	-23	-0.5	-1	-13	-0.3	+2	-5.5
LBN 52b	-1.5	0	-18	+4	+3	-9.5	+7	+2.5	

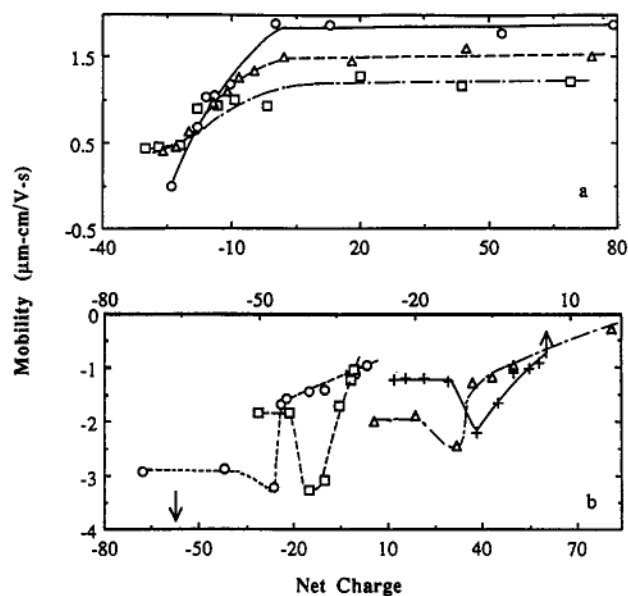
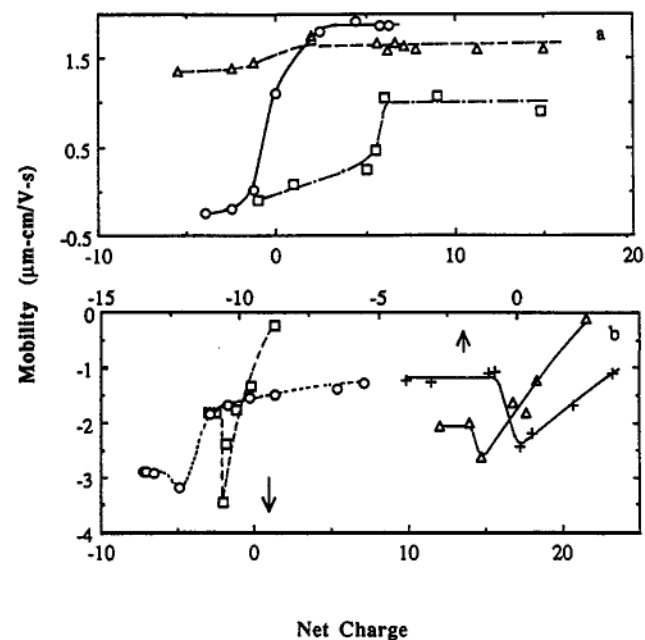
^a Z_c^q by QELS; Z_c^e by ELS.

TABLE IV: Range of Diameters (nm) of Soluble Complexes^a

polymer	BSA	RNase	lysozyme
polyanions			
NaPVS	6-45	6-46	6-48
NaPSS	46-63	46-60	46-57
PAMPS	30-110	30-85	30-98
NVP-AMPS	40-67	40-84	40-87
polycations			
PDMDAAC	20-48	20-68	20-87
LBN 52	28-81	28-88	28-75
LBN 66	31-87	31-86	31-99

^a The change of diameter from pH_c to pH₀.**Figure 7.** Electrophoretic mobility of RNase-LBN 66 in 0.10 M NaCl as a function of pH. Note the charge neutrality at the phase separation point. The mobility measurements at pH > pH₀ were made over a short time period on stable stirred suspensions and were stable and reproducible.**Figure 8.** Electrophoretic mobility of RNase with (a) PDMDAAC (Δ), LBN 66 (□), LBN 52 (○) and (b) PAMPS (□), NaPVS (○) (axis below); NaPSS (Δ) and NVP-AMPS (+) (axis above), all in 0.10 M NaCl.

Electrophoretic Light Scattering Study of the Complexation Process. The electrophoretic light scattering spectra obtained at four different angles for RNase-LBN 66 complex at pH 9.10 are shown in Figure 6. The average of the spectra gives a mobility of 0.7 (μm cm)/(V s). In contrast to QELS, ELS does not resolve a bimodal distribution at the complexation pH because the low charge and smaller size of the protein renders it "invisible". The mobility obtained at different pH is plotted in Figure 7. It is interesting to observe that there is no discontinuity in the plot at pH₀. This may suggest (a) that the mobility of the coacervate

**Figure 9.** Electrophoretic mobility of BSA with (a) PDMDAAC (Δ), LBN 66 (□), LBN 52 (○) and (b) PAMPS (□), NaPVS (○) (axis below); NaPSS (Δ) and NVP-AMPS (+) (axis above), all in 0.10 M NaCl.**Figure 10.** Electrophoretic mobility of lysozyme with (a) PDMDAAC (Δ), LBN 66 (□), LBN 52 (○) and (b) PAMPS (□), NaPVS (○) (axis below); NaPSS (Δ) and NVP-AMPS (+) (axis above), all in 0.10 M NaCl.

is the same as the mobility of the soluble aggregate with which it is in equilibrium or (b) that the charge:size ratio of the coacervate is too small for it to make a significant contribution to the measured mobility. In any event, one notes that the mobility of the complex starts decreasing around 9.10 as the pH progresses toward phase separation. When pH ≤ 9.10 the measured u values are identical to the mobility of LBN 66 polymer. The onset of the mobility change at pH 9.10 can be easily understood as a result of initial protein-polymer complexation by considering the motion of a complex in a electric field.

The motion of the complex at steady state in a field of strength E (V cm⁻¹) can be described by balancing the electrostatic force, F_e , and frictional force, F_f :

$$F_e = F_f \quad (13)$$

The electrostatic and frictional forces can be given by

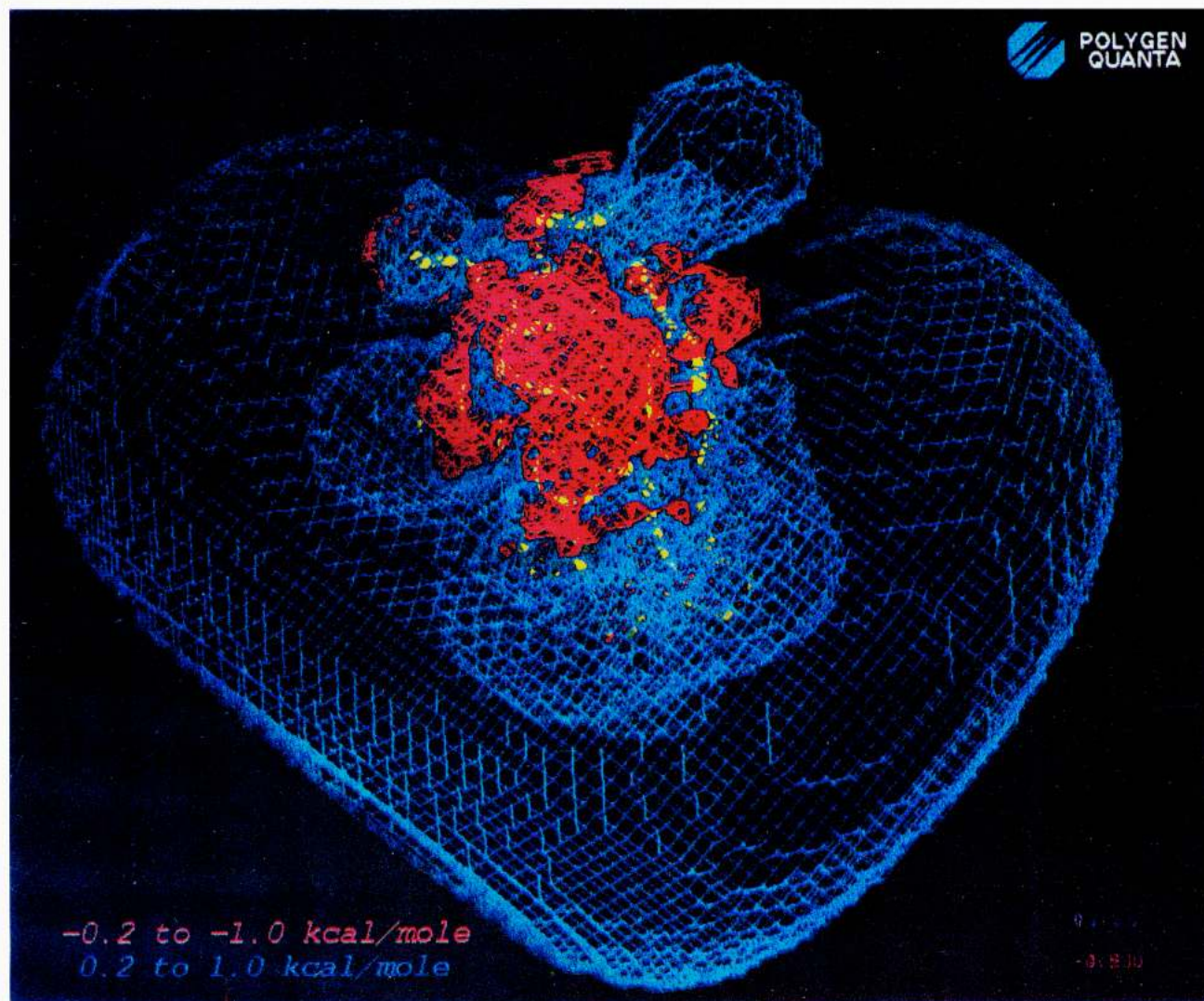


Figure 11. Electrostatic potential of RNase in solution calculated as described in text. The blue and red contours represent the potential ranges from 0.2 to 1.0 kcal/mol and from -0.2 to -1.0 kcal/mol, respectively; each range consists of five contour levels using an interval of 0.2 kcal/mol. The protein backbone is highlighted by a yellow ribbon. The view is looking down on to the protein active site. The protein has a large net positive charge at this pH, but the negative charge patch (red) is easily visualized.

$$F_c = (q_p + nq_{\text{pro}})E \quad (14)$$

$$F_f = v(f_p + \beta n f_{\text{pro}}) \quad (15)$$

where q_{pro} and q_p are the net charge of a bound protein and total polymer charge, respectively; f_{pro} and f_p are the friction coefficients of the bound protein and the polymer, respectively, which are assumed to combine additively; β is the friction coupling factor; E is the external field strength; v is the center-of-mass velocity of the complex; and n is the number of bound proteins per polymer chain. Substituting eqs 14 and 15 into eq 13, we have for the mobility of the complex

$$u = \frac{v}{E} = \frac{q_p + nq_{\text{pro}}}{f_p + \beta n f_{\text{pro}}} \quad (16)$$

The pH dependence of the complex mobility is expected from eq 14 since the net protein charge q_{pro} is a function of pH, as is n . Equation 16 is also reduced to the pure polymer mobility at $n = 0$. Therefore, the mobility change with pH may be used to characterize the initial protein–polyelectrolyte complexation via eq 16.

The plot of Figure 7, along with similar results for the other proteins and polyelectrolytes, is converted to mobility vs the net protein charge (Z) in Figures 8–10. Z , which is pH-dependent, is calculated from published pH titration curves.^{46–48} The net protein charge Z_c at initial binding for each of the protein–

polymer pairs from Figures 8–10 is also summarized in Table III. One notes that these results are consistent with the QELS data, and both QELS and ELS results obtained for the polyanions show that the higher the linear charge density the stronger the complexation. The effect of polyelectrolyte charge density on the complexation has been discussed elsewhere.²⁷

It is interesting to note the pronounced lack of symmetry for polyanions vs polycations in complex formation with proteins, as shown in Figures 8–10. Qualitatively, we can state that the linear charge densities, calculated by the Davis and Russell model,⁴⁴ of the polycations are in the order LBN52b > PDMDAAC \approx LBN66. For the polyanions, the sequence of linear charge densities is NVP-AMPS < PAMPS \approx NaPSS < PVS. Initially, we might have expected the curves to be centered about $Z = 0$, with Z_c for polyanions being approximately equal to $-Z_c$ for polycations of similar linear charge density. This is clearly not the case. Complex formation for proteins in the presence of polycations requires a negative net charge on the protein with a few exceptions; but in the presence of polyanions, complexation formation occurs even when the net charge of protein is of the same sign as the polyanion.

Previous turbidimetric and QELS studies of these protein–polyelectrolyte pairs also show that polyanions bind proteins more strongly than polycations even when the net protein charge is negative. This phenomenon can be understood in terms of nonuniform protein charge distribution or “surface charge

patches". This interpretation is supported by electrophoretic mobility data as shown by Figures 8–10, where the mobility becomes more negative when the proteins and polyanions initially interact. This change in mobility proves that the polyanions gain negative charge upon complexation. To overcome the global electrostatic repulsion, the proteins must have strong "positive charge patch" to bind the polymer units. From eq 16, the mobility gained at initial complexation also suggests that the initial complex does not have an increased friction factor relative to the free polymer. Therefore, an intra-polymer structure for the initial complexes is expected. For the few cases where the positive proteins associate with polycations, we did not observe the mobility increase at the point of initial binding. This could be a compensation of charge and friction effects.

The existence of nonuniform charge distribution or "surface charge patches" on the protein appears to play an important role in protein–polyelectrolyte interaction. An example of such patches is illustrated by the calculated electrostatic potential for RNase shown in Figure 11. Here the blue and red lines represent the ranges $e\psi = 0.2$ to 1.0 kcal/mol and $e\psi = -0.2$ to -1.0 kcal/mol contour levels, respectively. The amino acid sequence of RNase contains 18 basic and 10 acidic residues, of which 10 are lysine, 4 arginine, 4 histidine, 5 glutamic acid, and 5 aspartic acid. Given the side chain pK_a values of these residues, one can conclude that the fully charged condition would be most closely approached at pH 6, which is well below the isoelectric point (IEP) of RNase. As described in the Methods section, this is the amino acid representation we have used to calculate the electrostatic potential surrounding RNase. As one would expect at pH 6, RNase is seen to have a large positive net charge. However, even under these conditions, negatively charged areas still exist on the protein surface. How these surface charge patches change and redistribute as conditions are computationally varied is currently under investigation and will be communicated later.

With regard to the mechanism of phase separation, we proposed that at the point of coacervation

$$Z_T = Z_p + n_\phi Z_\phi = 0 \quad (17)$$

where Z_T is the net charge of the protein–polyelectrolyte complex, Z_p is the formal charge of the polyion, n_ϕ is the average number of protein molecules bound per polyion chain, and Z_ϕ is the protein net charge at the point of phase separation.¹⁶ The requirement of neutrality at phase separation is only observed here for complexes formed from polycations, as shown by the curves crossing zero mobility in Figures 8–10. For the polyanions, phase separation occur for complexes with a negative charge. Phase separation with polyanions seems complicated. Since soluble complexes exist only when the protein charge is between Z_c and Z_ϕ , the difference of $\Delta Z = |Z_c - Z_\phi|$ can be used to characterize the stability of the complexes. $\Delta Z_{BSA} > \Delta Z_{RNase} > \Delta Z_{lysozyme}$ are obtained for all polymers in Table III.

Conclusions

QELS and ELS are powerful techniques to study the interactions between polyelectrolytes and proteins. Both QELS and ELS results are consistent with a mechanism that entails an initial binding of polyelectrolytes to proteins localized at protein surface charge patches. Upon change in pH, the interaction between polyelectrolyte and proteins leads first to soluble complex formation and then to phase separation. It is suggested that a transition from intra-polymer to interpolymer complexation, followed by further aggregation, accompanies the progression from soluble complex to phase separation.

Acknowledgment. This research was supported by grants from the National Science Foundation (DMR 9014945), American Chemical Society (ACS-PRF No. 25532-AC7B), Eli Lilly Company, and Reilly Industries.

References and Notes

- (1) Sacco, D.; Bonneaux, F.; Dellacherie, E. *Int. J. Biol. Macromol.* **1988**, *10*, 305.
- (2) Dellacherie, E. *Am. Chem. Soc., Div. Polym. Chem. Prepr.* **1991**, *32* (1), 602 and references therein.
- (3) Lenk, T.; Thies, C. In *Coulombic Interactions in Macromolecular Systems*; Eisenberg, A., Bailey, F. E., Eds.; American Chemical Society: Washington, DC, 1987; Chapter 8.
- (4) Dubin, P.; Ross, T. D.; Sharma, I.; Yegelehner, B. In *Ordered Media in Chemical Separations*; Hinze, W. L., Armstrong, D. W., Eds.; American Chemical Society: Washington, DC, 1987; Chapter 8.
- (5) Veis, A. *Am. Chem. Soc., Div. Polym. Chem. Prepr.* **1991**, *32* (1), 596, and references therein.
- (6) Burgess, D. J.; Carless, J. E. *J. Colloid Interface Sci.* **1984**, *98*, 1.
- (7) Nguyen, T. Q. *Makromol. Chem.* **1986**, *187*, 2567.
- (8) Sternberg, M.; Hershberger, C. *Biochim. Biophys. Acta* **1974**, *342*, 195.
- (9) Kokufuta, E.; Shimizu, H.; Nakamura, I. *Macromolecules* **1981**, *14*, 1178.
- (10) Morawetz, H.; Hughes, W. L. *J. Phys. Chem.* **1952**, *55*, 64.
- (11) Berdick, M.; Morawetz, H. *J. Biol. Chem.* **1954**, *206*, 959.
- (12) Bozzano, A. G.; Andrea, G.; Glatz, C. E. *J. Membr. Sci.* **1991**, *55*, 181.
- (13) Clark, K. M.; Glatz, C. E. *Biotechnol. Prog.* **1987**, *3*, 241.
- (14) Fisher, R. R.; Glatz, C. E. *Biotechnol. Bioeng.* **1988**, *32*, 777.
- (15) Shieh, J.; Glatz, C. E. *Am. Chem. Soc., Div. Polym. Chem. Prepr.* **1991**, *32* (1), 606.
- (16) Stregre, M. A.; Dubin, P. L.; West, J. S.; Daniel Flinta, C. D. In *Protein Purification: from Molecular Mechanisms to Large-Scale Processes*; Ladisch, M., Willson, R. C., Painton, C. C., Builder, S. E., Eds.; American Chemical Society: Washington, DC, 1990; Chapter 5.
- (17) Burgess, R. R.; Jendrisak, J. *J. Biochemistry* **1975**, *14*, 4634.
- (18) Margolin, A.; Sheratyuk, S. F.; Izumrudov, V. A.; Zevin, A. B.; Kabanov, V. A. *Eur. J. Biochem.* **1985**, *146*, 625.
- (19) Ruckpoul, K.; Rein, H.; Janig, G. R.; Pfeil, W.; Ristau, O.; Damaschun, B.; Damaschun, H.; Muller, J. J.; Purschel, H. V.; Bleke, J.; Scheler, W. *Stud. Biophys.* **1972**, *34*, 81.
- (20) Regelson, W. *Interferon* **1970**, *6*, 353.
- (21) Ottenbrite, R. M.; Kaplan, A. M. *Annals New York Acad. Sci.* **1985**, *446*, 160.
- (22) (a) Kabanov, V. A.; Evdakov, B. P.; Mustafaev, M. I.; Antipina, A. D. *Mol. Biol.* **1977**, *11*, 582. (b) Kabanov, V. A.; Zevin, A. B. *Macromol. Chem. Suppl.* **1984**, *6*, 259.
- (23) Pecora, R. *Dynamic Light Scattering: Application of Photon Correlation Spectroscopy*; Plenum Press: New York, 1976.
- (24) Schmitz, K. S. *An Introduction to Dynamic Light Scattering by Macromolecules*; Academic Press: New York, 1990.
- (25) Kuil, M. E.; Mourik, F. V.; Burger, W.; Grondelle, R. V. *Biophys. Chem.* **1988**, *32*, 211.
- (26) Dubin, P. L.; Murrell, J. M. *Macromolecules* **1988**, *21*, 2291.
- (27) Park, J. M.; Muhoherac, B. B.; Dubin, P. L.; Xia, J. *Macromolecules* **1992**, *25*, 290.
- (28) Mabire, F.; Audebert, R.; Quivron, C. *Polymer* **1984**, *25*, 1317.
- (29) Wang, K. W.; Audebert, R. *J. Colloid Interface Sci.* **1988**, *131*, 32.
- (30) Subsequent elemental analysis of these dialyzed and freeze-dried NaPSS samples gave C:S ratios corresponding to 85–88% sulfonation.
- (31) (a) McQuigg, D. W. M.S. Thesis, Purdue University, 1991. (b) McQuigg, D. W.; Kaplan, J. I.; Dubin, P. L. *J. Phys. Chem.* **1992**, *96*, 1973.
- (32) Pecora, R.; Berne, B. J. *Dynamic Light Scattering*; Wiley: New York, 1976.
- (33) Stock, R. S.; Ray, W. H. *J. Polym. Sci., Polym. Phys. Ed.* **1985**, *23*, 1393.
- (34) Provencher, S. W. *Comput. Phys. Commun.* **1982**, *27*, 229.
- (35) Ware, B. R.; Haas, D. D. In *Fast Methods in Physical Biochemistry and Cell Biology*; Shaafi, R. I., Fernandez, S. M., Eds.; Elsevier: Amsterdam, 1983.
- (36) McQuarrie, D. A. *Statistical Mechanics*; Harper and Row: New York, 1976.
- (37) Ware, B. R. *Adv. Colloid Interface Sci.* **1974**, *4*, 1.
- (38) Polygen/Molecular Simulations Inc., 200 Fifth Ave. Waltham, MA 02154.
- (39) Brooks, B. R.; Brucoleri, R. E.; Olafson, B. D.; States, D. J.; Swaminathan, S.; Karplus, M. *J. Comput. Chem.* **1983**, *4*, 187.
- (40) Wlodawer, A.; Borkakoti, N.; Moss, D. S.; Howlin, B. *Acta Crystallogr., Sect. B* **1986**, *42*, 379.
- (41) Bernstein, F. C.; Koetzle, T. F.; Williams, G. J. B.; Meyer, Jr., E. F.; Brice, M. D.; Rodgers, J. R.; Kennard, O.; Shimanouchi, T.; Tasumi, M. *J. Mol. Biol.* **1977**, *112*, 535.
- (42) Brunger, A. T.; Karplus, M. *Proteins* **1988**, *4*, 148.
- (43) Davis, M. E.; Madura, J. D.; Luty, B. A.; McCammon, J. A. *Comput. Phys. Commun.* **1991**, *62*, 187.
- (44) Davis, R. M.; Russell, W. B. *J. Polym. Sci., Polym. Phys. Ed.* **1986**, *24*, 51.
- (45) Xia, J.; Dubin, P.; Dautzenberg, H. *Langmuir*, in press.
- (46) Tanford, C. *J. Am. Chem. Soc.* **1950**, *72*, 441.
- (47) Tanford, C.; Wagner, M. L. *J. Am. Chem. Soc.* **1954**, *76*, 3331.
- (48) Tanford, C.; Hauenstein, J. D. *J. Am. Chem. Soc.* **1956**, *78*, 5287.